Proceedings of the 11th World Congress on Mechanical, Chemical, and Material Engineering (MCM'25)

Paris, France - August, 2025 Paper No. ICMIE 183 DOI: 10.11159/icmie25.183

Design and Prototyping of a Stephenson Type III Mechanism for Repetitive Tasks with Symmetrical End-Effector Motion

Amani AlKhalaf, Fatemah Khalifah, Hawraa Ibrahim, Hebah Alazemi, Rawnaq Alfadhli, Ahmed Saber and Eddie Gazo-Hanna*

College of Engineering and Technology, American University of the Middle East Egaila 54200, Kuwait

56634@aum.edu.kw, 52474@aum.edu.kw, 59404@aum.edu.kw, 55647@aum.edu.kw, 59584@aum.edu.kw, ahmed.saber@aum.edu.kw, eddie-hanna@aum.edu.kw

Abstract - This paper investigates the kinematics of a novel Stephenson type III planar six-bar mechanism with one degree of freedom (DOF), integrating both four-bar and five-bar linkages. A detailed kinematic analysis is conducted by formulating closed-loop equations, with simulation results validated using SOLIDWORKS software. To ensure structural robustness, a static stress analysis is performed under expected operational loads, identifying critical stress points and confirming the design's adequacy. Furthermore, a physical prototype of the mechanism is developed to corroborate simulation outcomes and evaluate real-world performance. The results demonstrate the mechanism's suitability for compact, precise motion control, emphasizing its potential in diverse industrial and robotic applications.

Keywords: six-bar linkage; static analysis; robotics; planar mechanism.

1. Introduction

In recent years, parallel robotics and controllable mechanisms have been rapidly developed in mechanical engineering, and planar mechanisms have been widely used in contemporary design applications [1], [2], [3], [4], [5]. Among these, one-degree-of-freedom (DOF) six-bar mechanisms are particularly significant due to their ability to generate complex motion trajectories and force outputs using a relatively simple structure. These mechanisms consist of six interconnected links, including input and ground links, and are capable of executing a single input motion, while the remaining components follow a deterministic motion path.

Six-bar mechanisms with a single DOF can be broadly classified into two primary topologies: Watt's and Stephenson's mechanisms. Watt's six-bar linkage [6], [7] is widely recognized for converting rotary input into approximately linear motion and is commonly applied in steam engines, suspension systems, and robotic systems [8]. Watt's linkage includes two main variants: the traditional straight-line mechanism, used in guiding pistons along a linear path, and the Watt-I mechanism, which can be configured in up to eight distinct assembly modes [9].

In contrast, the Stephenson six-bar mechanism [7], [10] is structurally distinct, comprising one four-bar and one five-bar loop connected via two ternary links, which are separated by a binary link unlike the Watt linkage, where the ternary links are joined directly [8]. The Stephenson mechanism exists in three configurations. Stephenson I includes two ternary and four binary links and is employed in systems requiring a defined output path. Stephenson II consists of a ternary link, a quaternary link, and four binary links, making it suitable for applications demanding straight-line motion. Stephenson III features two quaternary and four binary links and is particularly well-suited for generating intricate motion paths, making it ideal for applications such as robotic joints, micromanipulators, and surgical instruments [9], [11], [12], [13], [14], [15].

The Stephenson III mechanism offers precise and repeatable motion within constrained workspaces, making it a viable solution in various high-precision industrial applications. It can be utilized in automated PCB assembly for high-speed, accurate component placement; as a micromanipulator mounted on the end-effectors of slower robotic arms for delicate operations; and in CNC milling and drilling machines for enhanced accuracy. Additionally, its refined motion control capabilities make it suitable for surface finish measurement systems, automated welding path tracking, and commercial

^{*}Corresponding author: eddie-hanna@aum.edu.kw

pick-and-place robots. In robotics, it can effectively replicate biologically inspired movements such as walking or swimming gaits. It also finds application in planar coordinate measuring machines where accurate and stable movement is essential.

This study focuses on a specific inversion of the Stephenson III mechanism, providing an in-depth analysis of its kinematic and dynamic characteristics to support its potential deployment in real-world applications. The kinematic analysis is conducted using the vector loop method, encompassing position, velocity, and acceleration evaluations for all links. Algebraic formulations are derived to describe the motion of the end effector, which are then validated through comparison with simulations performed in SOLIDWORKS.

The simulation results serve to visualize the mechanism's behavior and confirm the validity of the analytical models. The findings are discussed in detail to highlight key performance attributes and practical implications.

Following the kinematic assessment, the study proceeds with structural evaluation through static stress analysis at two critical crank positions using SOLIDWORKS. This step is essential to assess the mechanical integrity of the design under load. The stress distributions identify critical points susceptible to failure and help ensure that the design meets required safety and durability standards. To complement the theoretical and simulation-based investigations, a physical prototype of the mechanism was developed to experimentally validate the design.

2. Description of the Proposed Mechanism

The mechanism presented in Figure 1 represents a carefully selected planner six-bar linkage with a single degree of freedom. This configuration uniquely combines a four-bar linkage (O₂ABO₄) with a five-bar linkage (O₂ACDO₆), wherein the ternary link (ABC) functions as a shared component between both systems. To achieve optimal performance parameters, genetic algorithm optimization techniques were employed to establish the ideal dimensional specifications for each link. Through precisely controlled rotational movement of the driving crank (O₂A), the mechanism's designated point G effectively traces a specified planar trajectory with high precision.

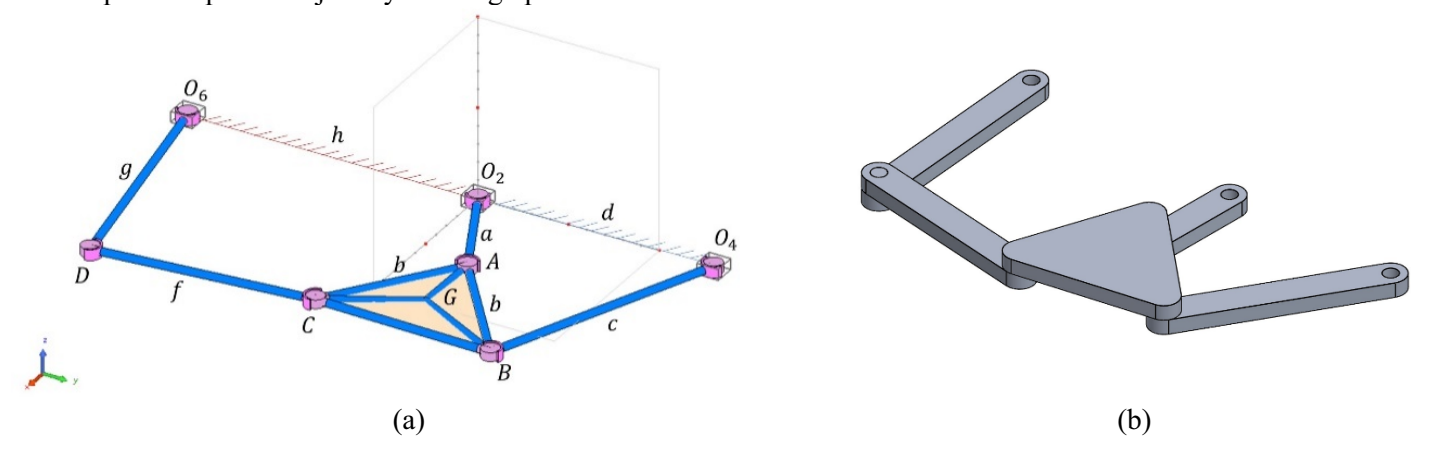


Fig. 1: (a) Scheme of the proposed mechanism, (b) Mechanism created using SOLIDWORKS.

3. Dimensional Synthesis

The dimensional synthesis process involves determining the optimal link lengths needed to produce a desired motion pattern. In this study, synthesis was performed using GIM software [16], [17] through a path generation approach, where the end effector is constrained to follow the specific trajectory within a planar workspace [18], [19], [20], as shown in Figure 2.

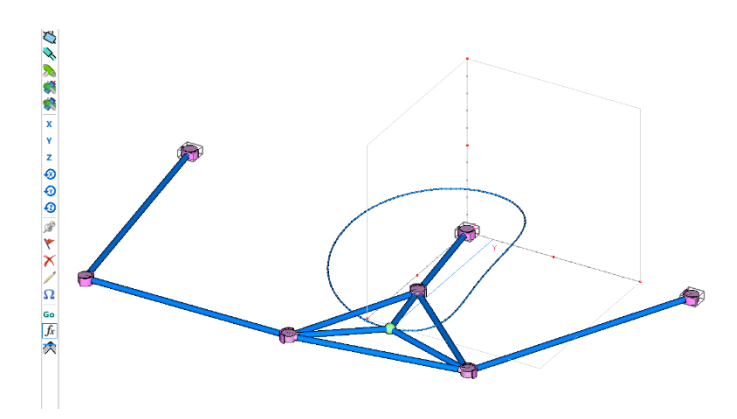


Fig. 2: Dimensional synthesis with desired path motion using GIM software.

The optimized dimensions obtained from this process are as follows:

a	62.6 mm		
ь	84.8 mm		
c	132 mm		
d	130 mm		
f	121mm		
g	136 mm		
h	170 mm		

45.7 mm

Table 1: Optimized dimensions of the proposed mechanism.

4. Kinematic Analysis

For the kinematic evaluation, calculations were performed based on the assumption of uniform crank angular velocity ($\omega_2 = 0.5 \text{ rad/s}$, $\alpha_2 = 0 \text{ rad/s}^2$). The analysis framework utilizes a Cartesian coordinate system (X-Y) established with its origin positioned at joint O_2 , as shown in Figure 3. Within this reference frame, each link's orientation is characterized by an angular measurement taken in the counterclockwise direction relative to the horizontal X-axis reference line. The six-bar mechanism was constructed within the SOLIDWORKS platform, featuring rectangular cross-section bars interconnected via cylindrical joint elements, as illustrated in Figure 4. The rectangular bars were dimensioned with a 20×10 mm profile, while the cylindrical connection pins were specified with a diameter of $\emptyset10\times10$ mm.

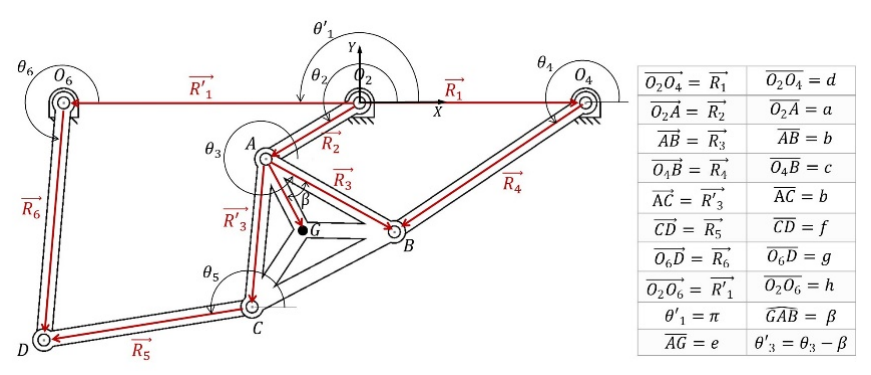


Fig. 3: Vector loops of the mechanism considered for synthesis.

4.1. Position Analysis

The vector loop equations of the four-bar O_2ABO_4 and for the five-bar O_2ACDO_6 mechanisms can be written as:

$$R_2 + R_3 - R_4 - R_1 = 0 ag{1}$$

$$R_2 + R_3 + R_5 - R_6 - R_1 = 0 (2)$$

The vector position equation of the end effector point G can be written in the form:

$$\vec{R}_G = \vec{O_2} A + \vec{A}G \tag{3}$$

By expanding the above expressions and separating the real and imaginary parts, we get the coordinates of the end-effector point G_X and G_V :

$$G_X = a\cos\theta_2 + e\cos(\theta_3 - \beta) \tag{4}$$

$$G_V = a\sin\theta_2 + e\sin(\theta_3 - \beta) \tag{5}$$

Figure 4 illustrates the trajectory traced by characteristic point G in the optimized design configuration, revealing a remarkably accurate and symmetrically balanced closed loop pattern. Comparative overlay of computational results derived from both MATLAB analytical formulations and SOLIDWORKS simulation environments demonstrates exceptional correlation, confirming the mathematical accuracy of the developed position analysis equations in predicting the mechanism's kinematic behavior.

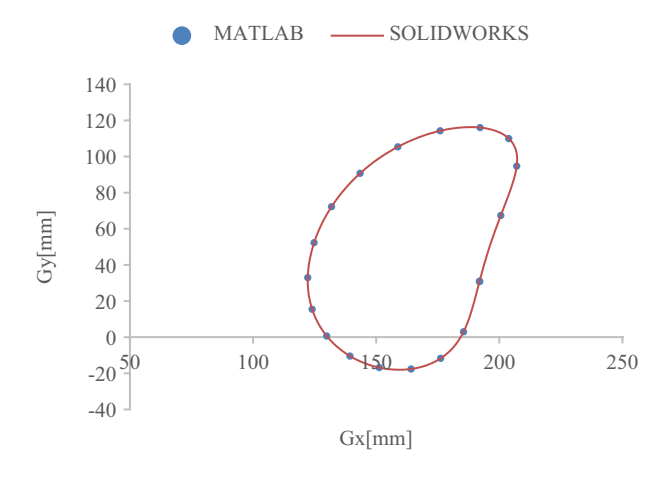


Fig. 4: Path of motion of the characteristic point G.

4.2. Velocity Analysis

To get an expression for the angular velocities of the different links as a function of the link lengths, the crank position, and the crank angular velocity, we differentiate equations (1) and (2) with respect to time.

$$ja\omega_2 e^{j\theta_2} + jb\omega_3 e^{j\theta_3} - jc\omega_4 e^{j\theta_4} = 0 \tag{6}$$

$$ja\omega_2 e^{j\theta_2} + jb\omega_3 e^{j\theta_3} - jf\omega_5 e^{j\theta_5} + jg\omega_6 e^{j\theta_6} = 0$$

$$\tag{7}$$

The velocity components of the end effector point G are calculated by numerical differentiation of the position equation (3):

$$v_{G_{v}} = -a \omega_{2} \sin \theta_{2} - e \omega_{2} \sin (\theta_{3} - \beta)$$
 (8)

$$v_{G_{\nu}} = a \,\omega_2 \cos \,\theta_2 + e \,\omega_3 \cos \left(\theta_3 - \beta\right) \tag{9}$$

Examination of the velocity characteristics presented in Figure 5 enables a comprehensive analysis of the velocity vector components associated with characteristic point G in the optimized six-bar planar mechanism. Analysis of Figure 5a reveals that the X-directional velocity component follows a sinusoidal distribution pattern that repeats consistently with crank angular position. This rhythmic velocity profile indicates fluid and gradual velocity transitions, a crucial characteristic for applications demanding high-precision motion control capabilities. Correspondingly, Figure 5b presents the Y-directional velocity component, which similarly exhibits sinusoidal behavioral characteristics. In both analytical representations, the remarkable congruence between MATLAB computational results and SOLIDWORKS simulation outputs provides robust validation that the theoretical mathematical models accurately reflect the physical behavior predicted by engineering simulation software.

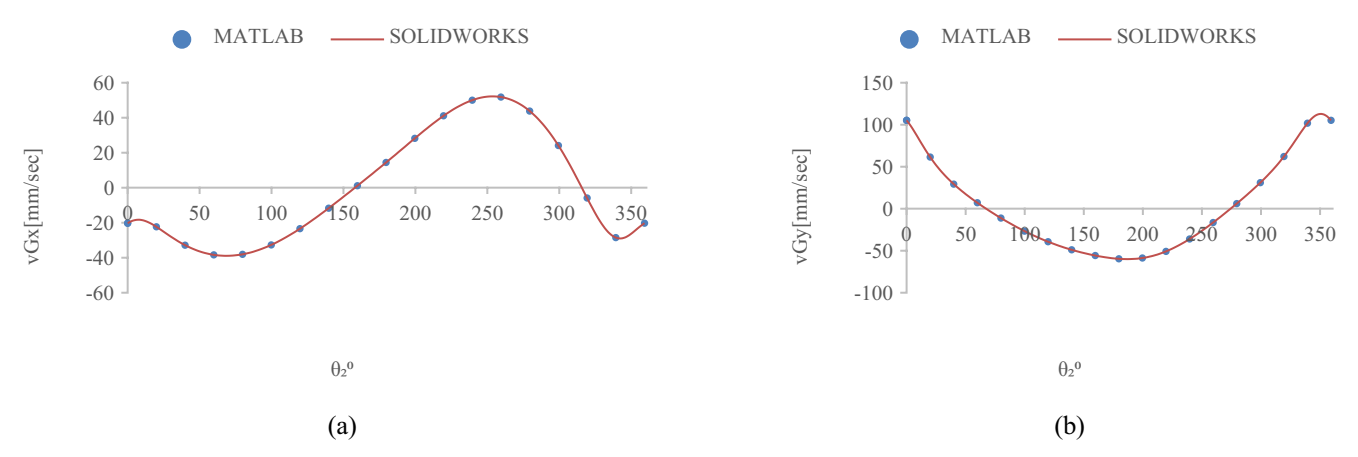


Fig. 5: Velocity of point G for the optimized design: (a) Direction 'X', (b) Direction 'Y'.

4.3. Acceleration Analysis

To get an expression for the angular accelerations of the different links as a function of the link lengths, the crank position, the crank angular velocity, and the crank angular acceleration, we differentiate equations (6) and (7) with respect to time.

$$\left(-a\omega_2^2 e^{i\theta_2}\right) + \left(b\alpha_3 j e^{i\theta_3} - b\omega_3^2 e^{i\theta_3}\right) - \left(c\alpha_4 j e^{i\theta_4} - c\omega_4^2 e^{i\theta_4}\right) = 0 \tag{10}$$

$$\left(a\alpha_{2}je^{j\theta_{2}}-a\omega_{2}^{2}e^{j\theta_{2}}\right)+\left(b\alpha_{3}je^{j\theta_{3}}-b\omega_{3}^{2}e^{j\theta_{3}}\right)+\left(f\alpha_{5}je^{j\theta_{5}}-f\omega_{5}^{2}e^{j\theta_{5}}\right)-\left(g\alpha_{6}je^{j\theta_{6}}-g\omega_{6}^{2}e^{j\theta_{6}}\right)=0\tag{11}$$

The acceleration components of the end effector point G are calculated by numerical differentiation:

$$a_{G_X} = -a\alpha_2\sin\theta_2 - a\omega_2^2\cos\theta_2 - e\alpha_3\sin(\theta_3 - \beta) - e\omega_3^2\cos(\theta_3 - \beta)$$
(12)

$$a_{G_V} = a\alpha_2 \cos \theta_2 - a\omega_2^2 \sin \theta_2 + e\alpha_3 \cos (\theta_3 - \beta) - e\omega_3^2 \sin (\theta_3 - \beta)$$
(13)

Figure 6 display the acceleration profiles of characteristic point G along the X-axis and Y-axis, respectively. Both analytical representations demonstrate exceptional concordance between computational results from MATLAB algorithms and

SOLIDWORKS simulation environments, validating the computational accuracy in predicting the mechanism's dynamic acceleration behavior.

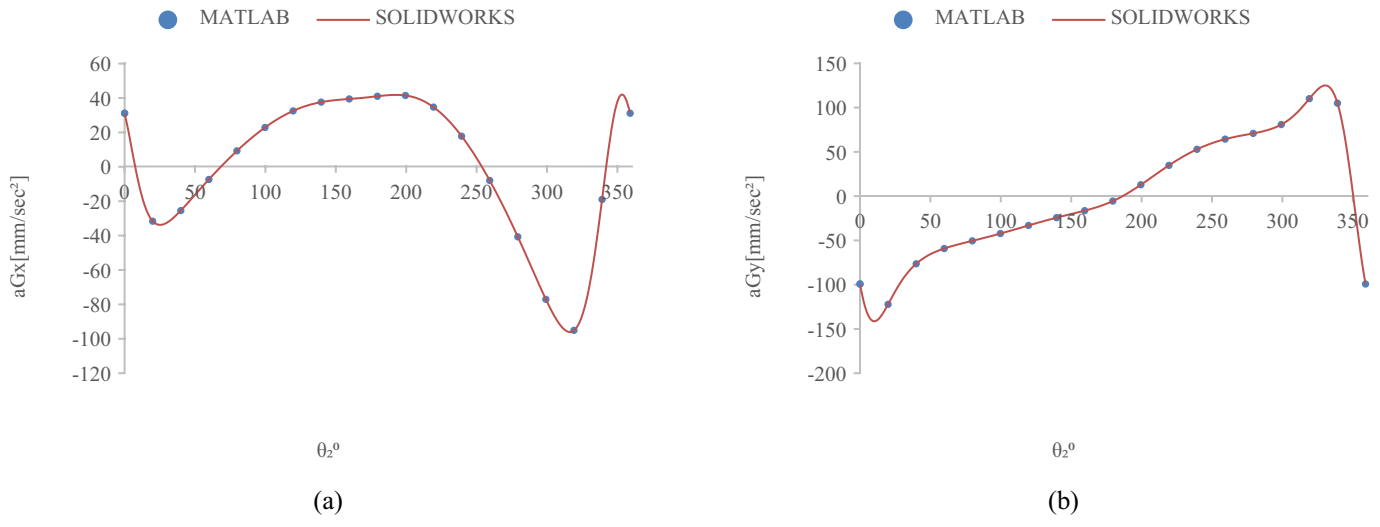


Fig. 6: Acceleration of point G for the optimized design: (a) Direction 'X', (b) Direction 'Y'.

5. Static Analysis

To ensure the structural reliability under operational loading, a static stress analysis was conducted to evaluate its ability to withstand external forces. The analysis was performed using the SOLIDWORKS simulation environment, which provided detailed predictions of stress distribution, deformation, and factor of safety. All interfacing components were defined with bonded contact conditions to simulate rigid, non-slipping joints under load, offering a conservative representation of the system's mechanical response. ABS thermoplastic was selected as the construction material for all links due to its strength, impact resistance, and compatibility with additive manufacturing; the corresponding material properties were sourced from the integrated SOLIDWORKS material database and are listed in Table 2. This simulation approach provided a comprehensive understanding of the mechanism's structural performance, validating the design's suitability for real-world applications subjected to moderate loading.

The boundary conditions for the simulation secured the mechanism at three critical hinge points: O_2 , O_4 , and O_6 . A vertically directed downward load was applied to represent a maximum operational load of 5 kg. Figure 7a illustrates the fixed constraint locations (highlighted in green) and the applied load vectors (shown in purple). The static stress analysis was specifically carried out at a crank angle of $\theta_2 = 270^\circ$, selected as the worst-case loading scenario due to the unfavorable alignment between the external load direction and the mechanism's geometry at this configuration. The computational domain was discretized using SOLIDWORKS' fine mesh setting, ensuring sufficient resolution for accurate stress predictions. The resulting finite element mesh consisted of 286,719 elements, as depicted in Figure 7b. This high-resolution mesh allowed for precise identification of stress concentrations and structural vulnerabilities across the mechanism.

Table 2: Mechanical properties of ABS.

Elastic Modulus	2000 MPa	Mass Density	1020 Kg/m ³
Poisson's Ratio	0.394	Tensile Strength	30 MPa
Shear Modulus	318.9 MPa	Yield Strength	32 MPa

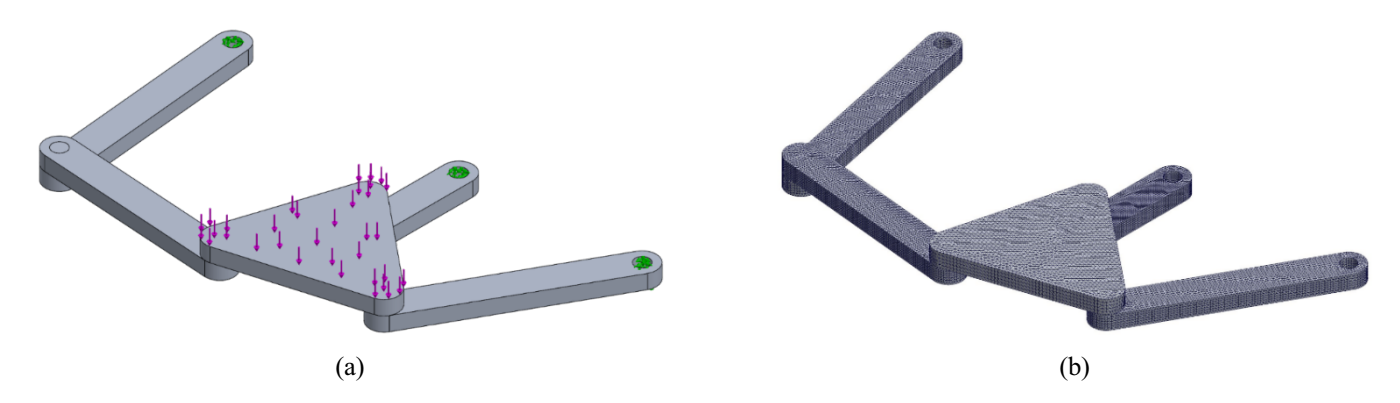


Fig. 7: (a) Load and fixtures, (b) Mesh structure.

The structural stress distribution throughout the mechanism is illustrated in Figure 8, based on maximum distortion energy theory, commonly referred to as the von Mises-Hencky theory. The simulation results indicate a maximum von Mises stress of 14.1 MPa, well below the yield strength of the material. In parallel, the deformation behavior of the mechanism under loading is depicted in Figure 9, with a maximum displacement of 3.61 mm observed at the most deflected region. To further assess the structural reliability, a factor of safety analysis was conducted, as shown in Figure 10. The calculated factor of safety, defined as the ratio of the material's yield strength to the maximum induced stress, is 2.27, confirming that the mechanism operates within a safe margin under the applied loading conditions.

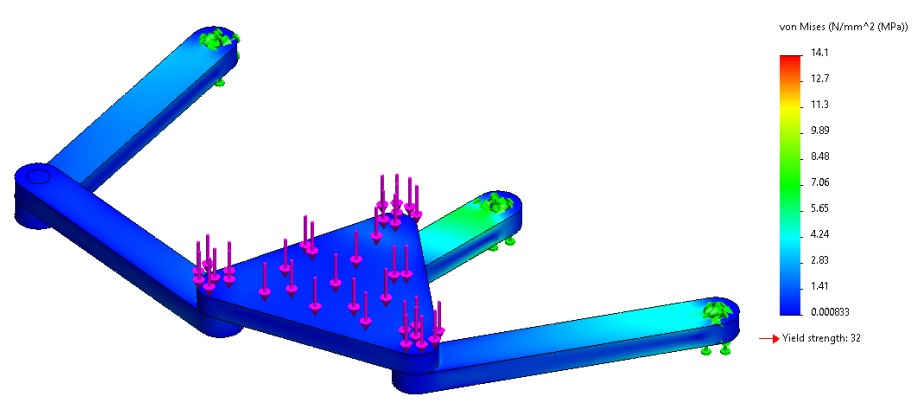


Fig. 8: Stress distribution.

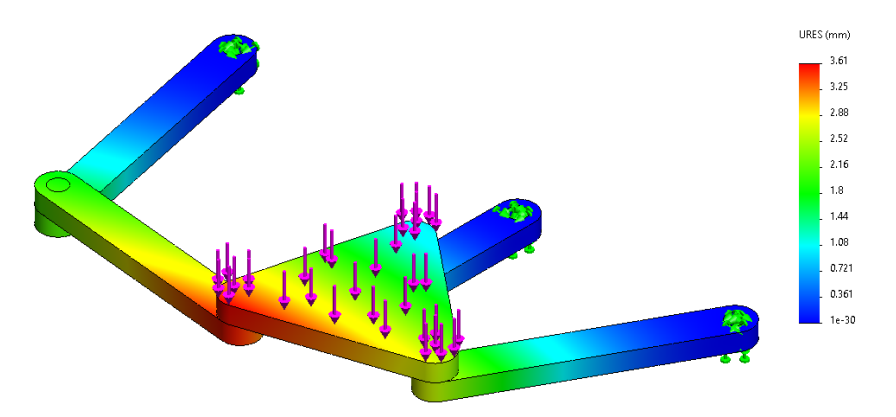


Fig. 9: Deformation distribution.

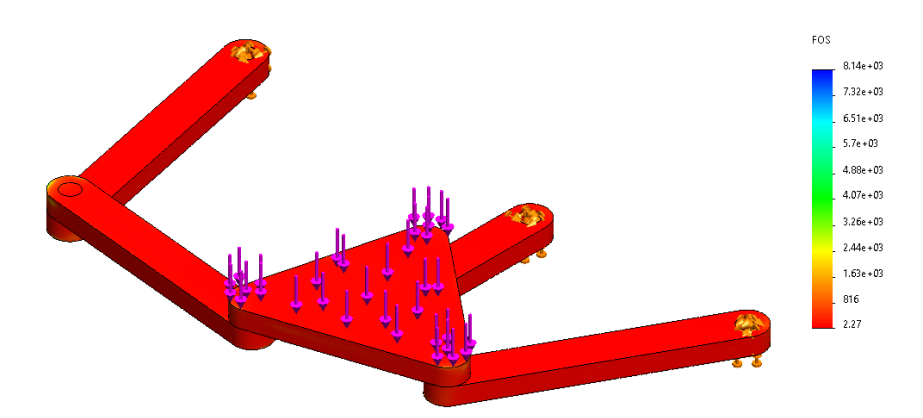


Fig. 10: Factor of safety distribution.

6. Prototype Development and Motion Verification

To experimentally validate the design, a physical prototype of the mechanism was fabricated using 3D-printed ABS thermoplastic, selected for its favorable balance of strength, durability, and ease of additive manufacturing. The assembly was mounted on a stable wooden base, and actuation was provided by a 12V DC motor operating at 5 RPM, connected to the input crank located at joint O₂. The prototype was constructed based on the optimized geometric parameters listed in Table 1 and exhibited smooth, symmetrical motion behavior, aligning closely with the kinematic simulation results. As illustrated in Figure 11, the observed motion confirms the practical feasibility of the proposed design and supports its applicability in tasks requiring compact, reliable, and repetitive end-effector movement.





Fig. 11: Prototype of the Mechanism during movement between different positions.

7. Conclusion

The novel Stephenson type III mechanism shows remarkable performance attributes when used for repetitive tasks that need precise symmetrical end-effector motion. The mechanism demonstrates outstanding concordance between simulated performance outcomes and theoretical models through thorough kinematic analysis and computational validation, and physical prototyping methods. The static stress analysis shows that the structure maintains sufficient integrity through safety factors between 2.835 and 8.169 at various operational positions. The mechanism delivers predictable symmetrical motion patterns combined with smooth velocity transitions, which proves essential in manufacturing and robotics applications because of their need for compact design and controlled movement. The mechanism achieves practical implementation readiness in industrial environments for reliable repetitive motion control thanks to optimized dimensional configuration derived through path generation methodology, which ensures desired motion characteristics and structural robustness.

Acknowledgements

The authors wish to acknowledge Erik Macho, Alfonso Hernández, CompMech, Department of Mechanical Engineering, UPV/EHU, for the permission to use the GIM® software. https://www.ehu.eus/compmech/software/

References

- [1] "Design and Analysis of Mechanisms: A Planar Approach | Wiley," Wiley.com. Accessed: May 14, 2024. [Online]. Available: https://www.wiley.com/en-jp/Design+and+Analysis+of+Mechanisms%3A+A+Planar+Approach-p-9781119054337
- [2] K. Zhao, J. P. Schmiedeler, and A. P. Murray, "Design of Planar, Shape-Changing Rigid-Body Mechanisms for Morphing Aircraft Wings," *Journal of Mechanisms and Robotics*, vol. 4, no. 041007, Sep. 2012, doi: 10.1115/1.4007449.
- [3] S. Amine, M. T. Masouleh, S. Caro, P. Wenger, and C. Gosselin, "Singularity analysis of the 4 RUU parallel manipulator using Grassmann-Cayley algebra," *Transactions of the Canadian Society for Mechanical Engineering*, vol. 35, no. 4, pp. 515–528, 2011, doi: 10.1139/tcsme-2011-0031.
- [4] S. Amine, L. Nurahmi, P. Wenger, and S. Caro, "Conceptual design of Schoenflies motion generators based on the wrench graph," presented at the Proceedings of the ASME Design Engineering Technical Conference, 2013. doi: 10.1115/DETC2013-13084.
- [5] S. Amine and E. Gazo Hanna, "Kinematic Analysis of HALF Parallel Robot," *Journal of Engineering Science and Technology Review*, vol. 12, pp. 207–213, Oct. 2019, doi: 10.25103/jestr.125.23.
- [6] H. Mehdigholi and S. Akbarnejad, "Optimization of Watt's Six-Bar Linkage to Generate Straight and Parallel Leg Motion," *International Journal of Advanced Robotic Systems*, vol. 9, p. 22, Jan. 2012, doi: 10.5772/50917.
- [7] M. S. Jo, J. K. Shim, H. S. Park, and W. R. Kim, "Dimensional Synthesis of Watt II and Stephenson III Six-Bar Slider-Crank Function Generators for Nine Prescribed Positions," *Applied Sciences*, vol. 12, no. 20, Art. no. 20, Jan. 2022, doi: 10.3390/app122010503.
- [8] J. Alvarez-Cedillo, T. Alvarez-Sanchez, and M. Aguilar-Fernandez, "Design of a Watt Mechanism with Crossed Axes," in *Telematics and Computing*, M. F. Mata-Rivera, R. Zagal-Flores, and C. Barria-Huidobro, Eds., Cham: Springer International Publishing, 2020, pp. 116–127. doi: 10.1007/978-3-030-62554-2 9.
- [9] G. R. Gogate and S. B. Matekar, "Unified synthesis of Watt-I six-link mechanisms using evolutionary optimization," *J Mech Sci Technol*, vol. 28, no. 8, pp. 3075–3086, Aug. 2014, doi: 10.1007/s12206-014-0715-0.
- [10] J. Hu, Y. Sun, and Y. Cheng, "High mechanical advantage design of six-bar Stephenson mechanism for servo mechanical presses," *Advances in Mechanical Engineering*, vol. 8, no. 7, p. 1687814016656108, Jul. 2016, doi: 10.1177/1687814016656108.
- [11] "Synthesis of WATT and Stephenson Mechanisms six bar mechanism using Burmester Theory Inpressco." Available: https://inpressco.com/synthesis-of-watt-and-stephenson-mechanisms-six-bar-mechanism-using-burmester-theory/
- [12] Y. Liu and S. Yang, "Kinematic solution of spherical Stephenson-III six-bar mechanism," *Chinese Journal of Mechanical Engineering*, vol. 26, pp. 851–860, Sep. 2013, doi: 10.3901/CJME.2013.05.851.
- [13] R. Singh, V. K. Pathak, A. Sharma, D. Buddhi, K. Saxena, P. Chander, D. Buddhi, and K. hazim Salem, "Caster Walker GAIT Trainer (CGT): A robotic assistive device," *Robot. Auton. Syst.*, vol. 159, no. C, Jan. 2023, doi: 10.1016/j.robot.2022.104302.
- [14] J. Wang, M. Yang, and Y. Huang, "The Kinematic Investigation of the Stephenson-III Spherical Mechanism with a Spherical Slider Containing a Spherical Prismatic Pair," *Applied Sciences*, vol. 13, no. 13, Art. no. 13, Jan. 2023, doi: 10.3390/app13137454.
- [15] S. Z. Ying, N. K. Al-Shammari, A. A. Faudzi, and Y. Sabzehmeidani, "Continuous Progressive Actuator Robot for Hand Rehabilitation," *Engineering, Technology & Applied Science Research*, vol. 10, no. 1, pp. 5276–5280, Feb. 2020, doi: 10.48084/etasr.3212.
- [16] V. Petuya, E. Macho, O. Altuzarra, C. Pinto, and A. Hernandez, "Educational software tools for the kinematic analysis of mechanisms," *Computer Applications in Engineering Education*, vol. 22, no. 1, pp. 72–86, 2014, doi: 10.1002/cae.20532.
- [17] E. Macho, M. Urízar, V. Petuya, and A. Hernández, "Improving Skills in Mechanism and Machine Science Using GIM Software," *Applied Sciences*, vol. 11, no. 17, Art. no. 17, Jan. 2021, doi: 10.3390/app11177850.
- [18] M. AlJaimaz, Z. AlMazidi, H. AlDousari, F. Ebrahem, D. AlZayyan, and E. Gazo Hanna, *Kinematic Analysis of a Variable Speed Deep Drawing Press Using GIM Software*. 2023. doi: 10.11159/icmie23.142.
- [19] S. Amine, B. Prasad, A. Saber, O. Mokhiamar, and E. Gazo-Hanna, "Design and Analysis of a Planar Six-Bar Crank-Driven Leg Mechanism for Walking Robots," *Applied Sciences*, vol. 14, no. 19, Art. no. 19, Jan. 2024, doi: 10.3390/app14198919.
- [20] E. Gazo-Hanna, A. Saber, and S. Amine, "Design and Modeling of a Six-Bar Mechanism for Repetitive Tasks with Symmetrical End-Effector Motion," *Engineering, Technology & Applied Science Research*, vol. 14, no. 5, pp. 16302–16310, 2024.